



Cite this: *RSC Adv.*, 2022, 12, 1149

Large improvement in thermoelectric performance of pressure-tuned Mg_3Sb_2 †

Juan Li, * Shuai Zhang, Kai Han, Bing Sun and Lianzhen Cao

The Mg_3Sb_2 -based Zintl compound is a promising candidate for a high-performance thermoelectric material with the advantage of the component elements being low cost, non-toxic and earth-abundant. Here, we investigate the influence of pressure on the electronic structure and p-type and n-type thermoelectric transport properties of Mg_3Sb_2 by using density functional theory and Boltzmann transport theory. The energy gaps first increase and then decrease with the increasing of pressure, and a peak value of the valley degeneracy of conduction band occurs at 4 GPa. Based on the calculated band structures, the zT (figure of merit) values of p-type Mg_3Sb_2 under pressure are significantly enhanced, which predominantly originates from the boosted PF (power factor) contributed by the increased carrier's relaxation time. When the carrier concentration reaches $1 \times 10^{20} \text{ cm}^{-3}$, the PF of p-type Mg_3Sb_2 at 4 GPa is increased by 35% relative to that of the compound at 0 GPa, thus leading to a considerably improved zT of ~ 0.62 at 725 K. Under the same conditions, due to the increased density of states effective mass, the n-type Mg_3Sb_2 exhibits a highest PF of $\sim 19 \mu\text{W cm}^{-1} \text{ K}^{-2}$ and a peak zT of 1.7. Therefore, pressure tuning is an effective method to improve the p-type and n-type thermoelectric transport performance of Mg_3Sb_2 -based Zintl compounds. This work on Mg_3Sb_2 under pressure may provide a new mechanism for the experimenters towards the enhancement of the thermoelectric performance of materials.

Received 8th December 2021
Accepted 23rd December 2021

DOI: 10.1039/d1ra08930g

rsc.li/rsc-advances

1. Introduction

More than half the energy content of the fuel is lost as waste heat. Thermoelectrics is an effective technology of directly interconverting heat and electrical energy without moving parts, which can be applied in power generation and solid-state refrigeration.^{1–5} Improving the energy conversion efficiency is the key factor influencing the extensive application of thermoelectric devices. The conversion efficiency is mainly governed by the performance of a thermoelectric material, which is quantified by the dimensionless figure of merit zT , $zT = S^2\sigma T/\kappa$, where S is the Seebeck coefficient, σ is the electrical conductivity, κ is the thermal conductivity and T is the absolute temperature.^{6–8} Therefore, increasing the power factor ($S^2\sigma$) or decreasing the κ are significant ways to improve the zT and thereby to enhance the energy conversion efficiency of the thermoelectric devices.^{9–12}

In addition to the thermoelectric material's performance, the cost and properties of the constituent elements also have an important influence on the widespread application of the thermoelectric technology. The advantage of the constituent

elements being low cost, non-toxic and earth-abundant make Mg_3Sb_2 -based Zintl compounds promising candidates for high-performance thermoelectric materials.^{13–15} By controlling the growing condition, Mg_3Sb_2 can exhibit not only p-type transport performance but also n-type transport performance.^{16–21} Pure Mg_3Sb_2 is an intrinsic p-type semiconductor ascribed to the Mg vacancy responsible for the p-type carriers.^{19,20,22} Song *et al.*²³ reported that through increasing the hole concentration, the zT value of 0.51 at 725 K can be achieved in p-type $\text{Mg}_{2.985}\text{Ag}_{0.015}\text{Sb}_2$. Due to the conduction band complexity, Mg_3Sb_2 exhibits more outstanding n-type thermoelectric performance. Based on a defect chemistry approach, Tamaki *et al.*²⁴ reported n-type $\text{Mg}_{3.2}\text{Sb}_{1.5}\text{Bi}_{0.49}\text{Te}_{0.01}$ with a high zT of 1.5 at 715 K, and similar results are reported by other groups.^{10,13,25–27}

Pressure tuning²⁸ is an effective strategy for designing high-performance thermoelectric materials through modifying the electronic structure. Under pressure, the lattice parameters and band gaps of materials will be significantly changed, which will result in some positive changes in the electronic structures.^{29,30} Because the key thermoelectric parameters (S and σ) are strongly dependent on the electronic structure, therefore, the strategy based on pressure tuning can be used to improve the thermoelectric performance of materials. Zhang *et al.*³¹ reported that the zT values of p-type SnSe along the b and c directions at 6 GPa and 700 K can be up to 2.5 and 1.7, respectively, and the zT of n-type sample at 600 K can reach 1.7. Polvani *et al.*³²

Department of Physics and Optoelectronic Engineering, Weifang University, Weifang 261061, China. E-mail: lj_wfu@163.com

† Electronic supplementary information (ESI) available. See DOI: 10.1039/d1ra08930g



reported that the zT value increased twofold in p-type $\text{Sb}_{1.5}\text{Bi}_{0.5}\text{Te}_3$ upon pressure tuning. For improving the thermoelectric performance of Mg_3Sb_2 , optimizing carrier concentration^{21,33–35} or tuning carrier scattering mechanism^{10,26} have been proved to be effective methods by a plenty of literatures, however, there are few theoretical reports about the method of pressure tuning. Therefore, it is necessary and important to investigate the effect of pressure on the thermoelectric properties of Mg_3Sb_2 , which can provide significant guides for the experimental researchers.

The intention of this work is therefore to study the electronic structures and thermoelectric properties of Mg_3Sb_2 at hydrostatic pressure by using first-principles calculations and Boltzmann transport theory. It is found that pressure tuning has a great influence on the band gap and valley degeneracy of Mg_3Sb_2 . Due to the positive changes in the electronic structure, the p-type and n-type thermoelectric properties of Mg_3Sb_2 are significantly improved. When the carrier concentration reaches $1 \times 10^{20} \text{ cm}^{-3}$, the zT of p-type Mg_3Sb_2 at 4 GPa and 725 K can be up to ~ 0.62 , $\sim 22\%$ higher than the value of the sample at 0 GPa, which predominantly originates from the considerably enhanced PF contributed by the increased carrier's relaxation

time. At the same temperature and carrier concentration, the n-type Mg_3Sb_2 at 4 GPa can exhibit a high PF of $\sim 19 \mu\text{W cm}^{-1} \text{ K}^{-2}$ and a peak zT of 1.7, which is mainly due to the increased density of states effective mass. These results demonstrate that pressure tuning is an effective way to the enhancement of the p-type and n-type thermoelectric transport properties of Mg_3Sb_2 -based Zintl compounds.

2. Computation methods

In this work, the density functional theory (DFT) combined with the projector augmented wave (PAW) method are carried out to calculate the electronic structures of Mg_3Sb_2 under different pressure, as implemented in the Vienna *Ab initio* Simulation Package (VASP).^{36–38} The optimized crystal parameters of Mg_3Sb_2 at 0 GPa can be obtained from our previous work.^{39,40} Under the pressure ranging from 1 to 10 GPa, the structural relaxation including the lattice constants and internal coordinates are allowed to relax into their equilibrium positions. The modified Becke Johnson functional of the Tran and Blaha (TB-mBJ) potential^{41,42} is adopted for obtaining the accurate electronic band structure. A $12 \times 12 \times 8$ Monkhorst-Pack k mesh,

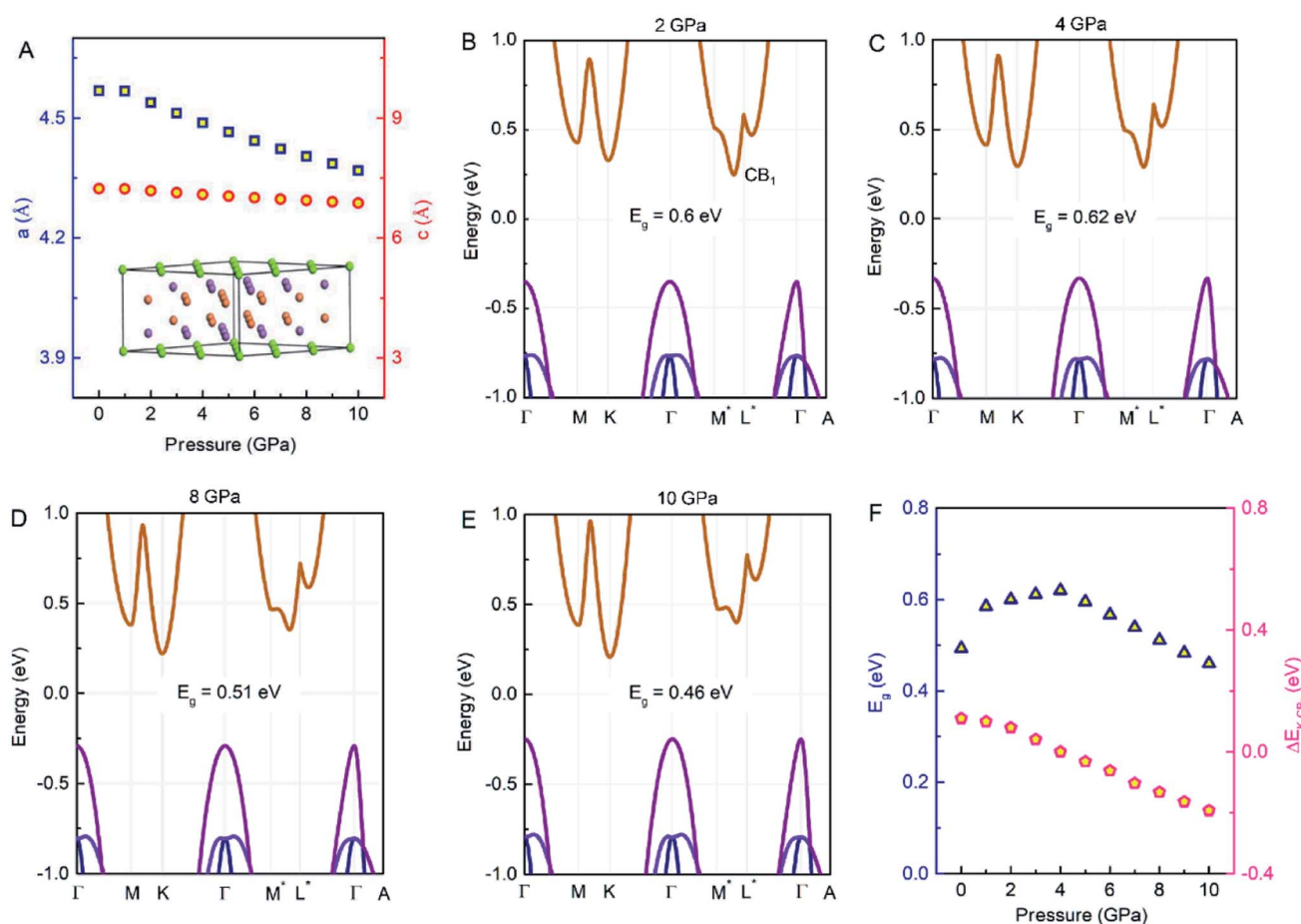


Fig. 1 (A) Lattice parameters a and c as a function of the pressure. The insert panel is the crystal structure of Mg_3Sb_2 , and the green, orange and purple balls represent Mg1, Mg2 and Sb atoms, respectively. (B–E) Calculated band structures of Mg_3Sb_2 with pressure being 2, 4, 8 and 10 (unit: GPa). (F) The energy gap E_g and the energy difference ΔE_{K-CB_1} between the K point in the band and CB_1 band point as a function of pressure.



a plane-wave cutoff energy of 400 eV and an energy convergence criterion of 10^{-4} eV are employed. Based on the calculated band structure, Effective Mass Calculator (EMC) program⁴³ is applied to calculate the effective masses. Considering that the spin orbit coupling (SOC) has an influence on the valence band of Mg_3Sb_2 ,⁴⁰ the calculated band structures with SOC are used for the following electronic transport calculations.

The semi-classic Boltzmann transport theory is applied to calculate the electronic transport properties based on the calculated band structure with SOC, as implemented in the BoltzTraP2 code.⁴⁴ The calculation results can directly present the temperature and carrier concentration dependence of S and σ/τ (where τ is the carrier's relaxation time). In order to obtain the σ , the deformation potential theory⁴⁵ is employed to calculate the τ and carrier mobility (μ). The minimum lattice thermal conductivity are evaluated using the Cahill's expression.⁴⁶

3. Results and discussion

The layered Zintl compound Mg_3Sb_2 crystallizes in an inverse α - La_2O_3 -type structure which belongs to the space group $P\bar{3}m1$, as displayed in Fig. 1A. This structure can be described as the cationic Mg^{2+} layers intercalated between the anionic $[\text{Mg}_2\text{Sb}_2]^{2-}$ layers. The Mg atoms in the ionic Mg^{2+} layers and in the covalently bonded $[\text{Mg}_2\text{Sb}_2]^{2-}$ layers are denoted as Mg1 and Mg2, respectively. The optimized lattice constants of

Mg_3Sb_2 at 0 GPa from our previous work^{39,40} are $a = 4.568$ Å and $c = 7.229$ Å. Fig. 1A shows the pressure dependence of the lattice parameters of Mg_3Sb_2 . In the pressure range of 0 to 10 GPa, the lattice parameters decrease as the pressure increases, and the decrease of a is larger than that of c . The changes of the lattice parameters may have a significant influence on the electronic structures, and further affect the thermoelectric properties of Mg_3Sb_2 .

The calculated band structures of Mg_3Sb_2 with pressure being 2, 4, 8 and 10 GPa are shown in Fig. 1B–E. With the pressure increasing, the valence band maximum at the Γ point move upward, and the conduction band minimum at the K point shift downward, whereas the conduction band minimum at the CB_1 point along the M^*-L^* line show an upward shift. When the pressure is below 4 GPa, the conduction band minimum is located at the CB_1 point, however, when the pressure continues to increase, the conduction band minimum is located at the K point. The energy gaps of Mg_3Sb_2 at 2, 4, 8 and 10 GPa are estimated to be 0.6, 0.62, 0.51 and 0.46 eV, respectively. In order to accurately describe the influence of pressure on the band gaps, the pressure dependence of the band gaps of Mg_3Sb_2 are shown in Fig. 1F. The band gaps present a first increase and then decrease trend with the increase of pressure. Changes in the band gaps may have an impact on the band effective mass. It is clearly that the pressure has a large effect on the conduction band energy difference $\Delta E_{K-\text{CB}_1}$ between the K

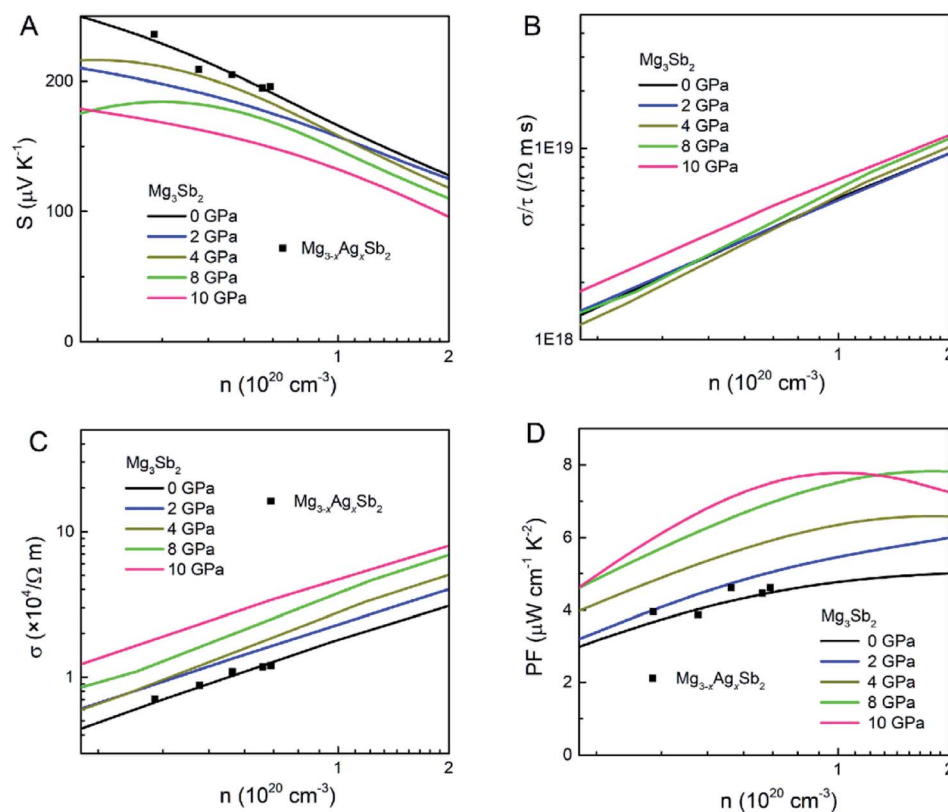


Fig. 2 The calculated (A) Seebeck coefficient S , (B) electrical conductivity with respect to relaxation time σ/τ , (C) electrical conductivity σ and (D) power factor PF as a function of carrier concentration n for p-type Mg_3Sb_2 at 725 K with pressure being 0, 2, 4, 8 and 10 (unit: GPa). The black squares are the experimental values of the reported $\text{Mg}_{3-x}\text{Ag}_x\text{Sb}_2$ from ref. 23.

Table 1 The calculated lattice elastic constant c_{11} (GPa), single valley effective mass m_s^* (m_e) of the Γ valence band, conductivity effective mass m_i^* (m_e) of the Γ valence band, the deformation potential Ξ (eV) of the valence band, and the carrier mobility μ ($\text{cm}^2 \text{V}^{-1} \text{s}^{-1}$) and relaxation time τ (fs) at 725 K for p-type Mg_3Sb_2 with pressure being 0, 2, 4, 8 and 10 (unit: GPa)

Pressure	c_{11}	m_s^*	m_i^*	Ξ	μ	τ
0	76.50 ^a	0.433	0.174	30.7	33.18	3.29
2	80.74	0.416	0.175	25.5	43.07	4.28
4	89.78	0.414	0.186	25.0	49.69	4.96
8	102.45	0.407	0.200	24.4	53.97	6.13
10	108.49	0.402	0.203	24.0	59.29	6.84

^a Ref. 40.

point in the band and CB_1 band point. As can be seen from Fig. 1F, with the increase of pressure, the absolute value of $\Delta E_{\text{K-CB}_1}$ decrease firstly and then increase. When the pressure increases to 4 GPa, $\Delta E_{\text{K-CB}_1}$ approaches to nearly zero, giving rise to a peak in the valley degeneracy ($N_v = 11$). Because the thermoelectric parameters are closely associated with the band effective mass and valley degeneracy, pressure tuning may be an effective way to achieve high-thermoelectric properties of Mg_3Sb_2 -based materials.

Fig. 2 shows the S , σ/τ , σ and PF as a function of carrier concentration for p-type Mg_3Sb_2 at 725 K with pressure being 0,

2, 4, 8 and 10 GPa, and the comparison with the experimental data of the reported $\text{Mg}_{3-x}\text{Ag}_x\text{Sb}_2$ sample. The calculated S consistent with the experimental value verifies the accuracy of our computation methods. The S of p-type Mg_3Sb_2 under different pressure has a negative relationship with the carrier concentration in certain doping range. At the same carrier concentration, the S calculated at 2, 4, 8 and 10 GPa are smaller than the value calculated at 0 GPa, which indicates that pressure tuning has a detrimental influence on the S of p-type Mg_3Sb_2 . In order to analyze the reason for the decrease of S under pressure, we calculate the single valley effective mass m_s^* of the Γ valence band based on the electronic band structure (see Table 1). The relationship between S and m_s^* is given by:⁴⁷

$$S = \frac{2k_B^2 T}{3e(h/2\pi)^2} N_v^{2/3} m_s^* \left(\frac{\pi}{3n} \right)^{2/3} \quad (1)$$

where m_s^* is the single valley effective mass, N_v is the valley degeneracy, n is the carrier concentration, T is the absolute temperature, h is the Planck constant and k_B is the Boltzmann constant. According to the equation, the S is in positive correlation with the density of states effective mass ($m_d^* = N_v^{2/3} m_s^*$). The m_s^* of the Γ valence band at 0, 2, 4, 8 and 10 GPa are estimated to be 0.433 m_e , 0.416 m_e , 0.414 m_e , 0.407 m_e and 0.402 m_e , respectively, which reveals that pressure tuning may lead to a decrease in the m_s^* of the Γ valence band. Due to the negligible effect of the pressure on the valley degeneracy of the Γ valence band (Fig. 1B–E), the decreased S of p-type Mg_3Sb_2 by pressure

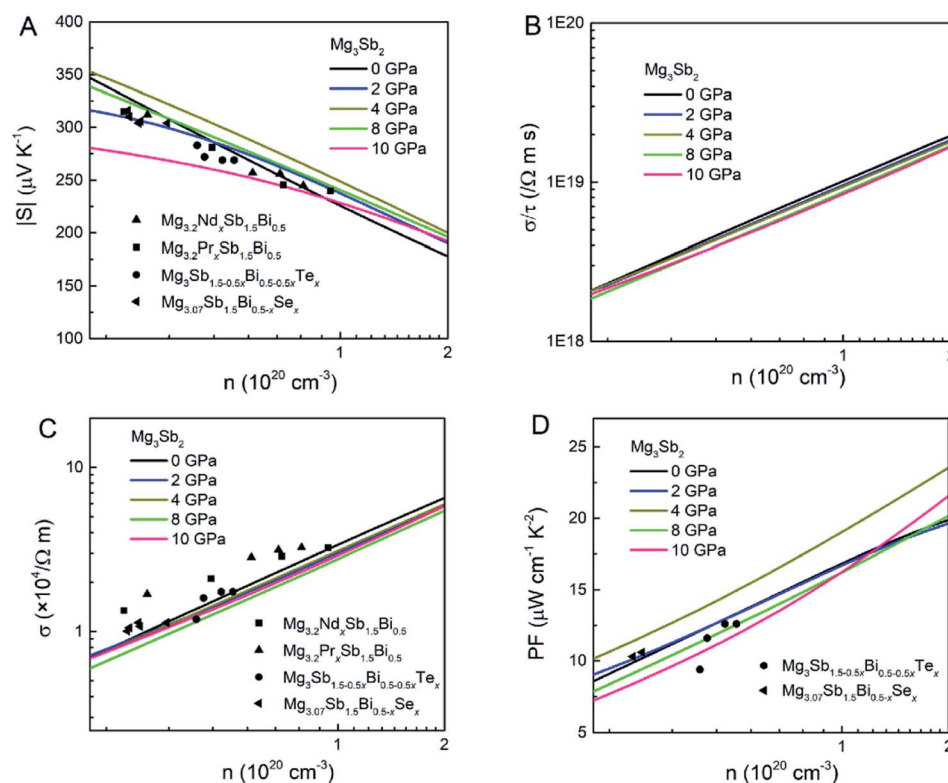


Fig. 3 The calculated (A) Seebeck coefficient S , (B) electrical conductivity with respect to relaxation time σ/τ , (C) electrical conductivity σ and (D) power factor PF as a function of carrier concentration for n-type Mg_3Sb_2 at 725 K with pressure being 0, 2, 4, 8 and 10 (unit: GPa). The experimental data of the n-type $\text{Mg}_{3.2}\text{Nd}_x\text{Sb}_{1.5}\text{Bi}_{0.5}$,³³ $\text{Mg}_{3.2}\text{Pr}_x\text{Sb}_{1.5}\text{Bi}_{0.5}$,²⁵ $\text{Mg}_3\text{Sb}_{1.5-0.5x}\text{Bi}_{0.5-0.5x}\text{Te}_x$ (ref. 14) and $\text{Mg}_{3.07}\text{Sb}_{1.5}\text{Bi}_{0.5-x}\text{Se}_x$ (ref. 13) samples are plotted for comparison.

tuning may be mainly ascribed to the decrease of the m_s^* of the Γ valence band.

As shown in Fig. 2B, the σ/τ of p-type Mg_3Sb_2 at 0, 2, 4, 8 and 10 GPa show an increasing trend as the carrier concentration increases. The τ for determining the σ can be estimated by the deformation potential theory, as expressed as:^{40,48}

$$\mu = \frac{2\sqrt{2\pi}e(h/2\pi)^4 c_{ii}}{3(k_B T)^{3/2} m_s^{*3/2} m_l^* \Xi^2} \quad (2)$$

$$\tau = \frac{\mu m_l^*}{e} = \frac{2\sqrt{2\pi}(h/2\pi)^4 c_{ii}}{3(k_B T m_s^*)^{3/2} \Xi^2} \quad (3)$$

where μ is the carrier mobility, m_s^* is the single valley effective mass, m_l^* is the conductivity effective mass, Ξ is the deformation potential, c_{ii} is lattice elastic constant, h is the Planck constant and k_B is the Boltzmann constant. The larger the value of c_{ii} and the smaller the values of m_s^* and Ξ , the better the performance of τ . Table 1 lists the input parameters and the calculated τ at 725 K for p-type Mg_3Sb_2 with pressure being 0, 2, 4, 8 and 10 GPa. With the increasing of pressure, the increased c_{11} and the decreased m_s^* and Ξ are beneficial to the τ . The τ at 0, 2, 4, 8 and 10 GPa are estimated to be 3.29, 4.28, 4.96, 6.13 and 6.84 fs, respectively. Based on the calculated τ , the σ as a function of carrier concentration for p-type Mg_3Sb_2 with pressure being 0, 2, 4, 8 and 10 GPa are plotted in Fig. 2C. At the same carrier concentration, because of the enhanced τ , there is an improvement in the σ with the increase of pressure. As a result of the largely improved σ , the theoretical PF for p-type Mg_3Sb_2 is strongly enhanced as the pressure increases (Fig. 2D). Because there may exist phase transition in Mg_3Sb_2 at pressure above 5 GPa,^{49,50} therefore, pressure tuning on p-type thermoelectric properties require careful selection of the pressure. When the carrier concentration increases up to $1 \times 10^{20} \text{ cm}^{-3}$, p-type Mg_3Sb_2 at 4 GPa exhibits a high PF of $\sim 6.2 \mu\text{W cm}^{-1} \text{ K}^{-2}$, 35% higher than the value of $\sim 4.6 \mu\text{W cm}^{-1} \text{ K}^{-2}$ for the compound at 0 GPa. Therefore, pressure tuning can make a significant contribution to the excellent p-type electronic transports for Mg_3Sb_2 -based compounds.

Fig. 3 shows the S , σ/τ , σ and PF as a function of carrier concentration for n-type Mg_3Sb_2 at 725 K with pressure being 0, 2, 4, 8 and 10 GPa, and the comparison with the experimental data of the reported Nd-, Pr-, Te- and Se-doped Mg_3Sb_2 -based compounds. The discrepancy between the simulated results and the experimental data is mainly ascribed to the effect of Bi doping on the electrical transport properties of Mg_3Sb_2 .³⁹ At the same carrier concentration, compared to the samples at 0, 2, 8 and 10 GPa, the n-type Mg_3Sb_2 at 4 GPa possesses a higher S . As can be seen from Table 2, with the increase of pressure, the m_s^* of the CB_1 conduction band (m_{s, CB_1}^*) increases, whereas the m_s^* of the K conduction band ($m_{s, \text{K}}^*$) decreases. Because of the smaller absolute value of $\Delta E_{\text{K-CB}_1}$ (below $\sim 0.11 \text{ eV}$) at 0, 2 and 4 GPa (Fig. 1F), the average m_s^* (0.252 m_e , 0.255 m_e and 0.257 m_e) of the both bands are used for calculating the τ . The increased m_s^* and the highest valley degeneracy (Fig. 2C) mainly contribute to the excellent S of n-type Mg_3Sb_2 at 4 GPa.

Table 2 Calculated single valley effective mass $m_{s, \text{K}}^*$ (m_e) of the K conduction band, single valley effective mass m_{s, CB_1}^* (m_e) of the CB_1 conduction band, conductivity effective mass $m_{l, \text{K}}^*$ (m_e) of the K conduction band, conductivity effective mass m_{l, CB_1}^* (m_e) of the CB_1 conduction band, the deformation potential Ξ (eV) of the conduction band, and the carrier mobility μ ($\text{cm}^2 \text{ V}^{-1} \text{ s}^{-1}$) and relaxation time τ (fs) at 725 K for n-type Mg_3Sb_2 with pressure being 2, 4, 8 and 10 (unit: GPa), in comparison with the previously reported values at 0 GPa

Pressure	$m_{s, \text{K}}^*$	m_{s, CB_1}^*	$m_{l, \text{K}}^*$	m_{l, CB_1}^*	Ξ	μ	τ
0	0.299 ^a	0.205 ^a	0.289 ^a	0.178 ^a	45.0 ^a	27.00 ^a	3.33 ^a
2	0.297	0.212	0.287	0.18	43.0	25.14	3.16
4	0.293	0.220	0.283	0.186	44.5	25.85	3.29
8	0.287	0.235	0.278	0.196	43.9	20.25	3.42
10	0.285	0.242	0.276	0.201	43.7	22.03	3.45

^a Ref. 40.

As shown in Table 2, the calculated τ for n-type Mg_3Sb_2 at 2, 4, 8 and 10 GPa are 3.16, 3.29, 3.42 and 3.45 fs, respectively. It is clearly that there is no obvious improvement in τ with the increasing of the pressure, which may be ascribed to the moderately changed μ according to the equation $\sigma = ne\mu$.³⁹ Based on the calculated τ using the deformation potential theory, the σ as a function of carrier concentration for n-type Mg_3Sb_2 at 725 K with pressure being 0, 2, 4, 8 and 10 GPa are plotted in Fig. 3C. The σ shows an increasing trend as the pressure increases. Owing to the not remarkably increased τ , the contribution of the pressure tuning to the σ is not significant. Combined the calculated S and σ , Fig. 3D presents the PF as a function of carrier concentration for n-type Mg_3Sb_2 under different pressure. The synergistic effect of the increased S and the moderately changed σ at 4 GPa make the n-type Mg_3Sb_2 possess the highest PF of $\sim 19 \mu\text{W cm}^{-1} \text{ K}^{-2}$ at the carrier concentration of $1 \times 10^{20} \text{ cm}^{-3}$. Therefore, further optimization of the electronic transport properties in n-type Mg_3Sb_2 -based materials can be expected through pressure tuning.

The κ is generally composed of the electronic thermal conductivity (κ_e) and lattice thermal conductivity (κ_l). The observed κ_l of Mg_3Sb_2 -based materials in the experiments can reach the minimum lattice thermal conductivity (κ_{min}).^{24,25,51} In order to investigate the effect of the pressure on the thermal

Table 3 The calculated bulk modulus B (GPa), shear modulus G (GPa), transversal velocity v_t (m s^{-1}), longitudinal velocity v_l (m s^{-1}), and the minimum lattice thermal conductivity κ_{min} ($\text{W m}^{-1} \text{ K}^{-1}$) for Mg_3Sb_2 with pressure being 2, 4, 8 and 10 (unit: GPa), in comparison with the previously reported values at 0 GPa

Pressure	B	G	v_t	v_l	κ_{min}
0	45.60 ^a	17.87 ^a	2107.68 ^a	4154.64 ^a	0.53 ^a
2	47.74	20.72	2247.47	4285.95	0.56
4	53.84	23.49	2350.34	4475.30	0.60
8	64.74	27.99	2491.03	4755.13	0.66
10	69.62	29.53	2526.50	4853.62	0.68

^a Ref. 40.



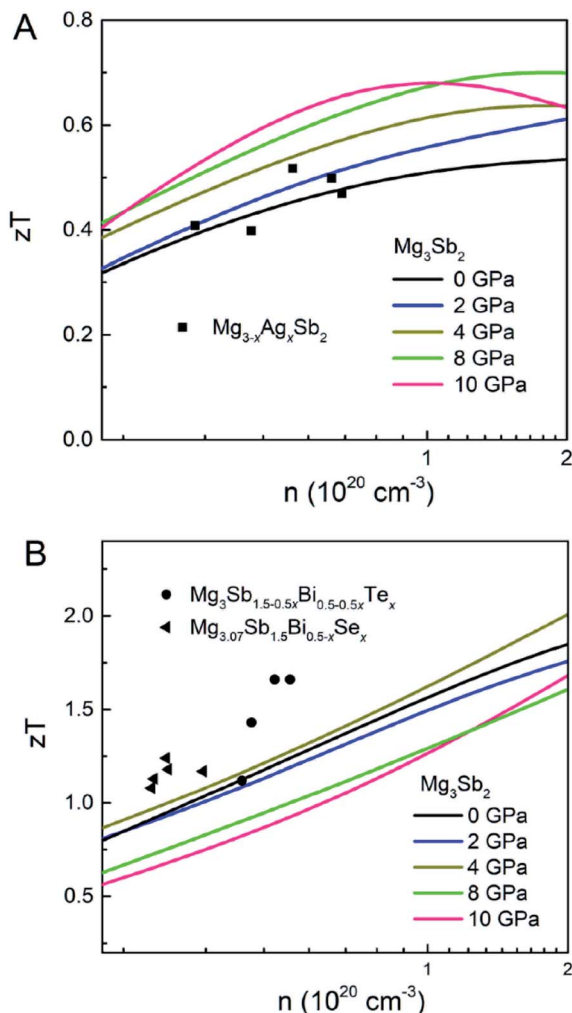


Fig. 4 The calculated zT as a function of carrier concentration for (A) p-type and (B) n-type Mg_3Sb_2 at 725 K with pressure being 0, 2, 4, 8 and 10 (unit: GPa). In (A), the black squares represent the previously reported p-type $\text{Mg}_{3-x}\text{Ag}_x\text{Sb}_2$.²³ In (B), the black circles and triangles represent the previously reported n-type $\text{Mg}_3\text{Sb}_{1.5-0.5x}\text{Bi}_{0.5-0.5x}\text{Te}_x$ and $\text{Mg}_{3.07}\text{Sb}_{1.5}\text{Bi}_{0.5-x}\text{Se}_x$.^{13,14}

transport performance, the κ_{\min} for Mg_3Sb_2 at different pressure are calculated using the Cahill's formula:^{39,40}

$$\kappa_{\min} = \frac{1}{2} \left(\frac{\pi}{6} \right)^{1/3} k_B (V)^{-2/3} (2\nu_s + \nu_l) \quad (4)$$

$$\nu_l = \sqrt{\frac{G}{\rho}} \quad (5)$$

$$\nu_s = \sqrt{\left(B + \frac{4}{3}G \right) / \rho} \quad (6)$$

where the ν_s and ν_l represent the transverse and longitudinal speed of sound, respectively, and the B and G denote the bulk and shear modulus, respectively. The input parameters and the calculated κ_{\min} are displayed in Table 3. These key parameters (ν_s , ν_l , B and G) increase with the increasing of the pressure, which is detrimental to the κ_{\min} of Mg_3Sb_2 . The κ_{\min} at 2, 4, 8

and 10 GPa are estimated to be 0.56, 0.60, 0.66 and 0.68 $\text{W m}^{-1} \text{K}^{-1}$, respectively, slightly higher than the value at 0 GPa (0.53 $\text{W m}^{-1} \text{K}^{-1}$). These results reveal that pressure tuning is not conducive to the reduction of the κ_{\min} of Mg_3Sb_2 -based compounds.

The experimental κ_e for p-type and n-type Mg_3Sb_2 at 725 K are in the range of 0.1–0.2 $\text{W m}^{-1} \text{K}^{-1}$ and 0.14–0.36 $\text{W m}^{-1} \text{K}^{-1}$, respectively.^{23,25,33,34,52} Here, the average κ_e (0.15 $\text{W m}^{-1} \text{K}^{-1}$ and 0.25 $\text{W m}^{-1} \text{K}^{-1}$ respectively for p-type and n-type sample) and the κ_{\min} are applied for estimating the κ . Based on the calculated PF and κ , Fig. 4 shows the simulated zT for p-type and n-type Mg_3Sb_2 at 725 K with pressure being 0, 2, 4, 8 and 10 GPa, and the comparison with the previously reported experimental data. As can be seen from Fig. 4A, the calculated zT of p-type Mg_3Sb_2 basically coincide with the experimental data, which demonstrates the correctness of the computational methods. It is found that the zT values of p-type Mg_3Sb_2 at 2, 4, 8 and 10 GPa are significantly improved compared to the value of the sample at 0 GPa. The largely enhanced thermoelectric performance of the sample by the pressure predominantly originates from the considerably increased PF. As a result, when the carrier concentration reaches $1 \times 10^{20} \text{ cm}^{-3}$, the p-type Mg_3Sb_2 at 4 GPa exhibits a peak zT of ~ 0.62 , $\sim 22\%$ higher than the value of the sample at 0 GPa. Compared to the experimental data, the underestimated zT of n-type Mg_3Sb_2 calculated by the DFT method can be ascribed to the neglect of the contribution of the Bi doping on the κ_1 and PF.^{6,39} (Fig. 4B). Among all samples, the Mg_3Sb_2 at 4 GPa shows the best n-type performance with a zT of 1.7 at the carrier concentration of $1 \times 10^{20} \text{ cm}^{-3}$, which is mainly resulting from the increased PF. Based on the above analysis, a conclusion can be drawn that the pressure tuning is an effective method to achieve an enhancement of not only p-type but also n-type thermoelectric performance of Mg_3Sb_2 -based Zintl compounds.

4. Conclusion

In this work, we have investigated the influence of the pressure on the electronic band structures and p-type and n-type thermoelectric transport properties of Mg_3Sb_2 by using the density functional theory and semi-classic Boltzmann transport theory. According to the calculated results of the band structure, increasing pressure can lead the energy gaps to first increase and then decrease, and the pressure of 4 GPa can contribute to a peak value of the valley degeneracy of the conduction band. Because of the increased τ , the PF of p-type Mg_3Sb_2 at 4 GPa and 725 K is increased by $\sim 35\%$ percent than that of the compound at 0 GPa, thus leading to a considerably enhanced zT of ~ 0.62 at the carrier concentration of $1 \times 10^{20} \text{ cm}^{-3}$. Besides its impact on the p-type transports, pressure tuning can also influence the n-type transports of Mg_3Sb_2 . When the pressure increases up to 4 GPa, the n-type sample at the carrier concentration of $1 \times 10^{20} \text{ cm}^{-3}$ can exhibit a high PF of $\sim 19 \mu\text{W cm}^{-1} \text{K}^{-2}$ and a peak zT of 1.7, resulting mainly from the increased density of states effective mass. Therefore, pressure tuning is an effective method to improve the p-type and n-type thermoelectric transport performance of Mg_3Sb_2 -based Zintl compounds. This work



on Mg_3Sb_2 under pressure may provide a new mechanism for experimenters to the enhancement of the thermoelectric performance of materials.

Conflicts of interest

There are no conflicts to declare.

References

- 1 L. E. Bell, *Science*, 2008, **321**, 1457–1461.
- 2 B. Jiang, Y. Yu, J. Cui, X. Liu, L. Xie, J. Liao, Q. Zhang, Y. Huang, S. Ning, B. Jia, B. Zhu, S. Bai, L. Chen, S. Pennycook and J. He, *Science*, 2021, **371**, 830–834.
- 3 J. Mao, H. Zhu, Z. Ding, Z. Liu, G. A. Gamage, G. Chen and Z. Ren, *Science*, 2019, **365**, 495–498.
- 4 S. Roychowdhury, T. Ghosh, R. Arora, M. Samanta, L. Xie, N. K. Singh, A. Soni, J. He, U. V. Waghmare and K. Biswas, *Science*, 2021, **371**, 722–727.
- 5 K. Imasato, C. Fu, Y. Pan, M. Wood, J. Kuo, C. Felser and G. J. Snyder, *Adv. Mater.*, 2020, **32**, 1908218.
- 6 K. Imasato, S. D. Kang, S. Ohno and G. J. Snyder, *Mater. Horiz.*, 2018, **5**, 59–64.
- 7 L. Zhao, G. Tan, S. Hao, J. He, Y. Pei, H. Chi, H. Wang, S. Gong, H. Xu, V. P. Dravid, C. Uher, G. J. Snyder, C. Wolverton and M. G. Kanatzidis, *Science*, 2016, **351**, 141–145.
- 8 C. Chang, D. Wang, D. He, W. He, F. Zhu, G. Wang, J. He and L. Zhao, *Adv. Energy Mater.*, 2019, **9**, 1901334.
- 9 Z. Bu, X. Zhang, B. Shan, J. Tang, H. Liu, Z. Chen, S. Lin, W. Li and Y. Pei, *Sci. Adv.*, 2021, **7**, eabf2738.
- 10 X. Chen, H. Wu, J. Cui, Y. Xiao, Y. Zhang, J. He, Y. Chen, J. Cao, W. Cai, S. J. Pennycook, Z. Liu, L. Zhao and J. Sui, *Nano Energy*, 2018, **52**, 246–255.
- 11 Q. Zhu, S. Song, H. Zhu and Z. Ren, *J. Power Sources*, 2019, **414**, 393–400.
- 12 J. Zhang, L. Song, G. K. H. Madsen, K. F. F. Fischer, W. Zhang, X. Shi and B. B. Iversen, *Nat. Commun.*, 2016, **7**, 10892.
- 13 J. Zhang, L. Song, S. H. Pedersen, H. Yin, L. T. Hung and B. B. Iversen, *Nat. Commun.*, 2017, **8**, 13901.
- 14 J. Zhang, L. Song, A. Mamakhel, M. R. V. Jørgensen and B. B. Iversen, *Chem. Mater.*, 2017, **29**, 5371–5383.
- 15 A. Bhardwaj, A. Rajput, A. K. Shukla, J. J. Pulikkotil, A. K. Srivastava, A. Dhar, G. Gupta, S. Auluck, D. K. Misra and R. C. Budhani, *RSC Adv.*, 2013, **3**, 8504.
- 16 C. L. Condrona, S. M. Kauzlarich, F. Gascoin and G. J. Snyder, *J. Solid State Chem.*, 2006, **179**, 2252–2257.
- 17 K. Imasato, S. D. Kang and G. J. Snyder, *Energy Environ. Sci.*, 2019, **12**, 965–971.
- 18 K. Imasato, S. Ohno, S. D. Kang and G. J. Snyder, *APL Mater.*, 2018, **6**, 016106–016111.
- 19 J. Li, S. Zhang, S. Zheng, Z. Zhang, B. Wang, L. Chen and G. Lu, *J. Phys. Chem. C*, 2019, **123**, 20781–20788.
- 20 S. Ohno, K. Imasato, S. Anand, H. Tamaki, S. D. Kang, P. Gorai, H. K. Sato, E. S. Toberer, T. Kanno and G. J. Snyder, *Joule*, 2018, **2**, 141–154.
- 21 Z. Ren, J. Shuai, J. Mao, Q. Zhu, S. Song, Y. Ni and S. Chen, *Acta Mater.*, 2018, **143**, 265–271.
- 22 X. Shi, X. Wang, W. Li and Y. Pei, *Small Methods*, 2018, **2**, 1800022.
- 23 L. Song, J. Zhang and B. B. Iversen, *J. Mater. Chem. A*, 2017, **5**, 4932–4939.
- 24 H. Tamaki, H. K. Sato and T. Kanno, *Adv. Mater.*, 2016, **28**, 10182–10187.
- 25 J. Li, F. Jia, S. Zhang, S. Zheng, B. Wang, L. Chen, G. Lu and L. Wu, *J. Mater. Chem. A*, 2019, **7**, 19316–19323.
- 26 J. Mao, J. Shuai, S. Song, Y. Wu, R. Dally, J. Zhou, Z. Liu, J. Sun, Q. Zhang, C. d. Cruz, S. Wilson, Y. Pei, D. J. Singh, G. Chen, C. W. Chu and Z. Ren, *Proc. Natl. Acad. Sci. U. S. A.*, 2017, **114**, 10548–10553.
- 27 X. Shi, T. Zhao, X. Zhang, C. Sun, Z. Chen, S. Lin, W. Li, H. Gu and Y. Pei, *Adv. Mater.*, 2019, **31**, 1903387.
- 28 J. F. Meng, D. A. Polvani, C. D. W. Jones, F. J. DiSalvo, Y. Fei and J. V. Badding, *Chem. Mater.*, 2000, **12**, 197–201.
- 29 S. D. Guo and J. L. Wang, *RSC Adv.*, 2016, **6**, 31272–31276.
- 30 L. Xu, Y. Zheng and J. C. Zheng, *Phys. Rev. B: Condens. Matter Mater. Phys.*, 2010, **82**, 195102.
- 31 Y. Zhang, S. Hao, L. D. Zhao, C. Wolverton and Z. Zeng, *J. Mater. Chem. A*, 2016, **4**, 12073–12079.
- 32 D. A. Polvani, J. F. Meng, N. V. C. Shekar, J. Sharp and J. V. Badding, *Chem. Mater.*, 2001, **13**, 2068–2071.
- 33 J. Li, S. Zhang, F. Jia, S. Zheng, X. Shi, D. Jiang, S. Wang, G. Lu, L. Wu and Z.-G. Chen, *Mater. Today Phys.*, 2020, **15**, 100269.
- 34 X. Tang, B. Zhang, X. Zhang, S. Wang, X. Lu, G. Han, G. Wang and X. Zhou, *ACS Appl. Mater. Interfaces*, 2020, **12**, 8359–8365.
- 35 J. Zhang, L. Song and B. B. Iversen, *ACS Appl. Mater. Interfaces*, 2021, **13**, 10964–10971.
- 36 P. E. Blöchl, *Phys. Rev. B: Condens. Matter Mater. Phys.*, 1994, **50**, 17953–17979.
- 37 G. Kresse and J. Hafner, *Phys. Rev. B: Condens. Matter Mater. Phys.*, 1993, **47**, 558–561.
- 38 G. Kresse and D. Joubert, *Phys. Rev. B: Condens. Matter Mater. Phys.*, 1999, **59**, 1758–1775.
- 39 J. Li, S. Zhang, B. Wang, S. Liu, L. Yue, G. Lu and S. Zheng, *J. Mater. Chem. A*, 2018, **6**, 20454–20462.
- 40 J. Li, S. Zheng, T. Fang, L. Yue, S. Zhang and G. Lu, *Phys. Chem. Chem. Phys.*, 2018, **20**, 7686–7693.
- 41 D. J. Singh, *Phys. Rev. B: Condens. Matter Mater. Phys.*, 2010, **82**, 205102.
- 42 F. Tran and P. Blaha, *Phys. Rev. Lett.*, 2009, **102**, 226401.
- 43 A. Fonari and C. Sutton, *Effective Mass Calculator*, 2012, <http://github.com/afonari/emc>.
- 44 G. K. H. Madsen, J. Carrete and M. J. Verstraete, *Comput. Phys. Commun.*, 2018, **231**, 140–145.
- 45 J. Bardeen and W. Shockley, *Phys. Rev.*, 1950, **80**, 72–80.
- 46 D. G. Cahill, S. K. Watson and R. O. Pohl, *Phys. Rev. B: Condens. Matter Mater. Phys.*, 1992, **46**, 6131–6140.
- 47 R. Santos, S. A. Yamini and S. X. Dou, *J. Mater. Chem. A*, 2018, **6**, 3328–3341.
- 48 T. Fang, S. Zheng, T. Zhou, L. Yan and P. Zhang, *Phys. Chem. Chem. Phys.*, 2017, **19**, 4411–4417.



- 49 M. Calderón-Cueva, W. Peng, S. M. Clarke, J. Ding, B. L. Brugman, G. Levental, A. Balodhi, M. Rylko, O. Delaire, J. P. S. Walsh, S. M. Dorfman and A. Zevkink, *Chem. Mater.*, 2021, **33**, 567–573.
- 50 S. Ding, R. Su, W. Cui, J. Hao, J. Shi and Y. Li, *ACS Omega*, 2020, **5**, 31902–31907.
- 51 S. W. Song, J. Mao, M. Bordelon, R. He, Y. M. Wang, J. Shuai, J. Y. Sun, X. B. Lei, Z. S. Ren, S. Chen, S. Wilson, K. Nielsch, Q. Y. Zhang and Z. F. Ren, *Mater. Today Phys.*, 2019, **8**, 25–33.
- 52 J. Shuai, Y. Wang, H. S. Kim, Z. Liu, J. Sun, S. Chen, J. Sui and Z. Ren, *Acta Mater.*, 2015, **93**, 187–193.

